c. 1

DETECTION EFFICIENCY OF PLASTIC SCINTILLATORS FOR ELASTICALLY SCATTERED POSITIVE PIONS

by

LARRY THOMAS FELAWKA

B.Sc., University of Manitoba, 1968

A THESIS SUBMITTED IN PARTIAL FULFILMENT OF

THE REQUIREMENTS FOR THE DEGREE OF

MASTER OF SCIENCE

in the Department

of

Physics

We accept this thesis as conforming to the required standard

The University of British Columbia

April, 1973

ABSTRACT

The efficiency for detecting positive pions which have been scattered elastically from a target has been calculated for low pion energies. Measurements of the efficiency at pion kinetic energies 12 - 77 MeV were made for a 12" long x 5" diameter NE110 plastic scintillator optically coupled to a Philips XP1040 photomultiplier tube. The efficiencies varied from 94% at 12 MeV to 79% at 77 MeV.

TABLE OF CONTENTS

LIST OF TABLES

LIST OF FIGURES

ACKNOWLEDGEMENTS

I would like to take this opportunity to express my thanks to my research supervisor, Dr. David A. Axen, for his encouragement and assistance.

I should also like to thank Dr. C.H.Q. Ingram for his helpful observations and information.

CHAPTER I

INTRODUCTION

In order to distinguish between positive pions which have been scattered elastically from composite nuclei and those which have scattered inelastically either the momentum or the energy of both the incident and the scattered pions must be measured. The most convenient technique for determining the incident momentum is magnetic analysis. Elastically scattered pions can be identified as well if instead of measuring the momentum either the velocity (time of flight) or the energy deposited while passing through some material is measured.

The time-of-flight technique has limited usefulness for low-energy pions, as the path length required to measure the velocity accurately is usually large compared to the mean decay length of the pions, resulting in large particle loss. A second limitation is the reduction of the solid angle of scattering by the long flight path.

The pion energy can be conveniently measured by stopping the pions in a plastic scintillator and measuring the pulse height (or charge) produced by a photomultiplier tube optically coupled to the scintillator. Better energy resolution is obtained by stopping the pions completely rather than allowing them to pass through a relatively thin scintillator. Plastic scintillators are preferable to sodium iodide crystals because the short rise time ($\sim$ 5 nsec) of the pulses produced reduces background from random events during the pulse integration and hence improves overall resolution. The small range of the pions in plastic scintillator (about

10 cm for 50 MeV pions) allows the fabrication of relatively small and inexpensive detectors.

Monoenergetic pions which enter the stopping counter do not produce pulses all of the same height. The following processes will lead to deviations from the mean pulse height:

1) inelastic reactions in the scintillator

2) finite pulse integration time

3) pion decay before stopping in the scintillator.

The efficiency for detecting elastically scattered monoenergetic pions is defined as

$$\varepsilon = \frac{\text{counts in elastic peak}}{\text{total number of counts}} \tag{1}$$

Calculations of ε are made in Chapter II. Upper limits to small effects such as beam contamination by decay muons and elastic scattering of pions out of the scintillator are made in Chapter III. In Chapter IV experimental measurements of the efficiency for energies 12 to 77 MeV are described.

CHAPTER II

CALCULATION OF EFFICIENCY

Events are lost from the peak in the pulse height spectrum primarily because of the following processes:

1) pions undergo inelastic reactions with the ^{12}C nuclei before stopping

2) events are lost because of the finite pulse integration time

3) pions decay to muons before stopping.

If P_1, P_2 and P_3 are the respective probabilities that processes 1-3 do <u>not</u> occur, the efficiency is given by

$$\varepsilon = P_1 P_2 P_3 \tag{2}$$

1. Losses from Inelastic Reactions

The procedure used to calculate losses due to reactions is similar to that used by Measday and Richard-Serre[1,2] to calculate losses of protons in various types of materials. The probability of nuclear interaction in a slice of material of thickness ds, composed of n chemical elements is, by definition

$$\sum_{i=1}^{n} \sigma_i n_{Ai}$$

where $\sigma_i \equiv$ total reaction cross section for the i^{th} element

$n_{Ai} \equiv$ number of atoms of i^{th} element per unit area.

Also, $n_{Ai} = n_{vi} ds$, where n_{vi} is the number of atoms of the i^{th} element per unit volume.

The probability of interaction dP at a distance s in the scintillator is the product of the probability that no interaction has occurred in the distance s and the probability that the interaction occurs in the interval ds. Thus,

$$dP = (1-P) \sum_{i=1}^{n} \sigma_i(s) n_{vi} \, ds$$

The cross section has been written as $\sigma_i(s)$ to stress the fact that the cross section varies greatly with distance.

Integrating,

$$P = 1 - \exp\left[- \int_0^{S_R} \sum_{i=1}^{n} \sigma_i(s) n_{vi} \, ds \right]$$

where $S_R \equiv$ maximum penetration of π^+.

The probability of no interaction P_1 is thus

$$P_1 = \exp\left[- \int_0^{S_R} \sum_{i=1}^{n} \sigma_i(s) n_{vi} \, ds \right]$$

Changing the variable of integration from s to kinetic energy E

$$\int_0^{S_R} \sum_{i=1}^{n} \sigma_i(s) n_{vi} \, ds = \int_{E_0}^{0} \frac{\sum_{i=1}^{n} \sigma_i(E) n_{vi} \, dE}{\frac{dE}{ds}}$$

where $E_0 \equiv$ kinetic energy of incident particles

$$\therefore \quad P_1 = \exp\left[- \int_0^{E_0} \frac{\sum_{i=1}^{n} \sigma_i(E) n_{vi} \, dE}{\left| \frac{dE}{ds} \right|} \right] \tag{3}$$

The quantity $\frac{dE}{ds}$ for a material composed of a single element is given by the formula of Bethe[3]

$$\frac{dE}{ds} = - \frac{4\pi e^4 z^2 n_v Z}{m_0 c^2 \beta^2} \ln \left[\frac{2 m_0 c^2 \beta^2}{I(1-\beta^2)} - \beta^2 \right]$$

where $e \equiv$ elementary charge (e.s.u.)

$z \equiv$ charge number of incident particle

$n_v \equiv$ number of atoms of element/unit volume

$Z \equiv$ atomic number of element

$m_0 \equiv$ electron mass

$c \equiv$ speed of light in a vacuum

$\beta \equiv$ particle speed/c

$I \equiv$ geometric mean ionization potential of the element

Assuming complete additivity, then for a material composed of n elements

$$\frac{dE}{ds} = - \sum_{i=1}^{n} \frac{4\pi e^4 z^2 n_{v_i} Z_i}{m_0 c^2 \beta^2} \ln \left[\frac{2 m_0 c^2 \beta^2}{I_i(1-\beta^2)} - \beta^2 \right] \qquad (4)$$

Using the relativistic expression for kinetic energy,

$$E = M_0 c^2 \; [(1-\beta^2)^{-1/2} - 1] \qquad (5)$$

where M_0 = particle mass

we may express β^2 as

$$\beta^2 = \frac{\alpha(2+\alpha)}{(1+\alpha)^2} \qquad \text{where } \alpha \equiv \frac{E}{M_0 c^2}$$

Also, $n_{vi} = \frac{\rho f_i N_0}{M_i}$

where $\rho \equiv$ density of material

$f_i \equiv$ fraction of i^{th} element by weight

$N_0 \equiv$ Avogadro's number

$M_i \equiv$ gram atomic weight of i^{th} element

Substituting in (4),

$$\frac{dE}{ds} = -\rho \sum_{i=1}^{n} f_i a_i \left[\frac{(1+\alpha)^2 \ln[b_i \alpha(2+\alpha)]}{\alpha(2+\alpha)} - 1 \right] \tag{6}$$

Using the values[4]

$e = 4.80298 \times 10^{-10}\ cm^{3/2}\ g^{1/2}\ s^{-1}$

$z(\text{pions}) = 1$

$N_0 = 6.02252 \times 10^{23}$

$m_0c^2 = 0.511006$ MeV

$Z(^{12}C) = 6$

$M(^{12}C) = 12.01115$ g [5]

$I(^{12}C) = 78$ eV[5]

$Z(H_2) = 2$

$M(H_2) = 2.01594$ g

$I(H_2) = 18.7$ eV[5]

the constants a and b were calculated to be 0.153396 MeV $g^{-1}\ cm^2$ and

13102.7, respectively, for ^{12}C and 0.304649 MeV g^{-1} cm^2 and 54653.1, respectively, for H_2.

Equation (6) does not hold for small energies; the contribution to integral in eq. (3) below 0.1 MeV is small and was neglected. Thus,

$$P_1 \simeq \exp\left[-\int_{0.1}^{E_0} \frac{\sum_{i=1}^{n} \sigma_i(E)\, n_{vi}\, dE}{\frac{dE}{ds}}\right]$$

The reaction cross section for π^+ on ^{12}C as a function of pion kinetic energy in the range 0 - 100 MeV was obtained by fitting a polynomial to the available cross section data[6,7]. Experimental cross sections and the linear fit are shown in Fig. 1. At these energies there is no inelastic scattering of π^+ from protons. The ^{12}C cross section included excitation of the 4.4 MeV level of ^{12}C, as the resolution was insufficient to separate this contribution.

The density of NE110 plastic scintillator is 1.032 g cm^{-3} and the molecular formula is $CH_{1.104}$[8]. The fraction of ^{12}C by weight (f_1) is therefore 0.9152 and the fraction H_2 (f_2) is 0.0848.

Table I lists the values of P_1 calculated from equation (3).

2. <u>Losses Due to Finite Pulse Integration Time</u>

Pions decay in the following manner:

$$\pi^+ \xrightarrow{\tau_1 = 26\ \text{ns}} \mu^+ + \nu_\mu$$

$$\mu^+ \xrightarrow{\tau_2 = 2200\ \text{ns}} e^+ + \nu_e + \bar{\nu}_\mu$$

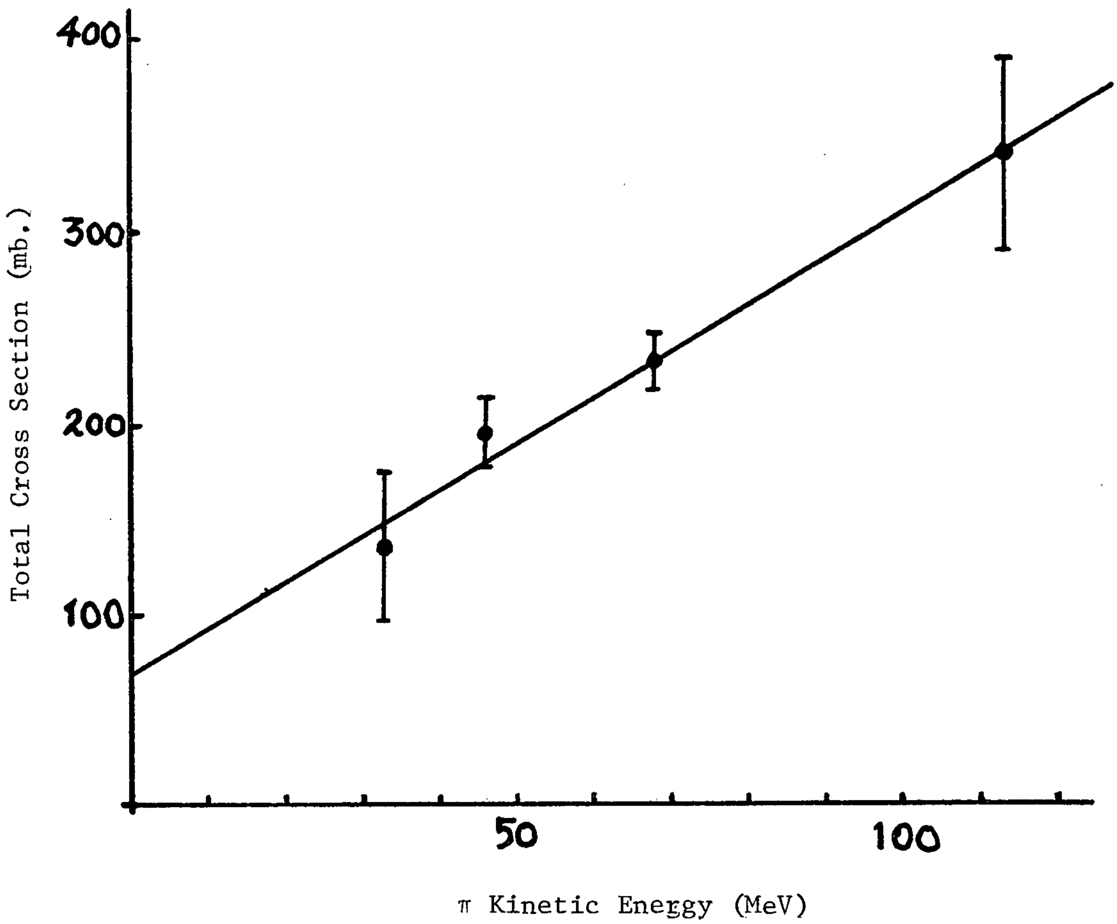

FIG. 1. Inelastic Reaction Cross Sections for π on ^{12}C

TABLE I

Probability P_1 of π^+ Stopping in Scintillator Without Undergoing Inelastic Reactions

Pion Kinetic Energy (MeV)	P_1
10	.998
20	.991
30	.981
40	.967
50	.948
60	.920
70	.883
80	.832
90	.763
100	.673
110	.564
120	.440
130	.312
140	.194
150	.103

Pions which come to rest before decaying will yield monoenergetic muons of kinetic energy 4.1 MeV (see Appendix A). The full energy peak in the analogue-to-digital converter (ADC) spectrum will correspond to an energy equal to the sum of the initial pion kinetic energy and the decay muon kinetic energy of 4.1 MeV. As the pulse is integrated for a finite time, a certain fraction of the pions will not have decayed during that time and a certain fraction will have decayed with a subsequent muon decay. Both of these cases result in loss of events from the peak in the ADC spectrum. The fraction of events corresponding to a pion decay but no muon decay within the integration time T was calculated in the following manner:

Using set theory notation, the following sets were defined:

$A \equiv \{$set of all events such that π^+ decays in the time interval $(t_1, t_1+dt_1)\}$

$B \equiv \{$set of all events such that μ^+ decays in the time interval $(t_2, t_2+dt_2)\}$

From the definition of conditional probability,

$$P(A \cap B) = P(A)P(B|A)$$

where $P(A \cap B) \equiv$ probability that both A and B occur

$P(A) \equiv$ probability that A occurs

$P(B|A) \equiv$ probability that B occurs, given that A occurs

Since the decay times t_1 and t_2 are both exponentially distributed,

$$P(A) = \frac{e^{-t_1/\tau_1}\, dt_1}{\tau_1}$$

$$P(B|A) = \frac{e^{-(t_2-t_1)/\tau_2}\,dt_2}{\tau_2}$$

where τ_1, τ_2 are the mean lifetimes of the π^+ and μ^+ respectively.

$$\therefore\ P(A \cap B) \equiv dP_2 = \frac{e^{-t_1/\tau_1}\,e^{-(t_2-t_1)/\tau_2}\,dt_1\,dt_2}{\tau_1\tau_2}$$

The integration was performed in the shaded region indicated in Fig. 2. In this region the pion has decayed and the muon has not.

$$\therefore\ P_2 = \int_T^\infty dt_2 \int_0^T \frac{e^{-t_1/\tau_1}\,e^{-(t_2-t_1)/\tau_2}\,dt_1}{\tau_1\tau_2}$$

$$= \frac{\tau_2\left(e^{-T/\tau_2} - e^{-T/\tau_1}\right)}{\tau_2 - \tau_1}$$

P_2 was plotted as a function of T (using τ_1 = 26.024 ns and τ_2 = 2199.4 ns[9]) in Fig. 3.

The highest efficiency is obtained when P_2 is a maximum. Setting $\frac{dP_2}{dT} = 0$ and solving for T, one obtains

$$T_{max} = \frac{\tau_1\tau_2 \ln\left(\frac{\tau_2}{\tau_1}\right)}{\tau_2 - \tau_1} = 117\ \text{ns}$$

$$P_{max} = \left(\frac{\tau_1}{\tau_2}\right)^{\frac{\tau_1}{\tau_2-\tau_1}} = 0.948$$

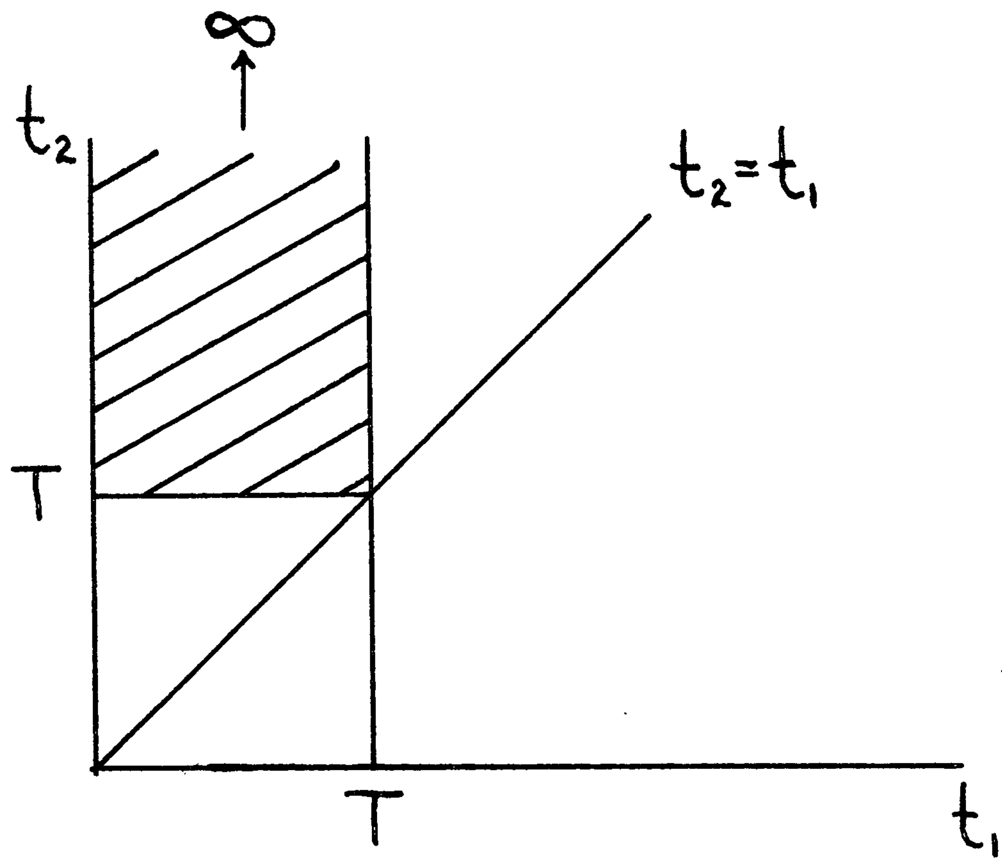

FIG. 2. Region of Integration of Probability Density Function

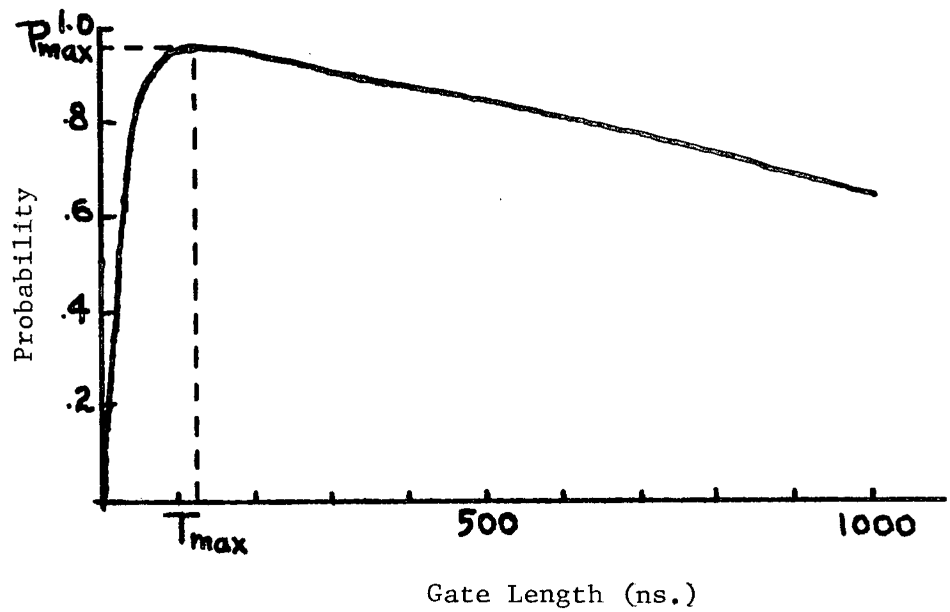

FIG. 3. Probability P_2 vs. Gate Length

3. Loss Due to Pion Decay before Stopping

The probability that the pion decays in the time interval $(t', t'+dt')$ is given by

$$dP = \frac{e^{-t'/\tau}\,dt'}{\tau}$$

where $\tau \equiv$ mean lifetime of π^+.

In this expression t' represents the time in the rest frame of the π^+. If the stopping time of the π^+ in the rest frame of the π^+ is T'_s, then the probability P_3 that the π^+ does not decay before stopping is

$$P_3 = \int_{T_s'}^{\infty} \frac{e^{-t'/\tau}\,dt'}{\tau} = e^{-T_s'/\tau} \qquad (7)$$

T'_s was calculated in the following manner:

By definition,

$$c\beta = \frac{ds}{dt}$$

where $t \equiv$ time in lab frame

$$\therefore\ c\beta = \frac{ds}{dE}\cdot\frac{dE}{d\beta}\cdot\frac{d\beta}{dt'}\cdot\frac{dt'}{dt}$$

From Eq. (5),

$$E = M_o c^2\left[(1-\beta^2)^{-1/2} - 1\right]$$

$$\frac{dE}{d\beta} = \beta M_o c^2 (1-\beta^2)^{-3/2}$$

Also, from relativistic time dilation,

$$\frac{dt'}{dt} = (1-\beta^2)^{1/2}$$

$$\therefore\ dt' = \frac{\beta M_o c^2 (1-\beta^2)^{-1}\,d\beta}{c\beta\,\frac{dE}{ds}}$$

Integrating,

$$T_s' = \frac{M_o c^2}{c} \int_{\beta_o}^{0} \frac{d\beta}{(1-\beta^2)\,\frac{dE}{ds}}$$

where β_0 corresponds to the initial π^+ velocity.

The above integration was performed numerically with M_0c^2 = 139.576 MeV. Eq. (6) was used to evaluate $\frac{dE}{ds}$.

The results of the calculation of P_3 using eq. (7) are given in Table II.

4. Total Efficiency

The efficiency was calculated from eq. (2); results are given in Table III and are plotted (along with experimental efficiencies) in Fig. 4. For this calculation, the assumption was made that the scintillator was large enough to contain pions which were scattered elastically from the ^{12}C and the ^{1}H nuclei in the scintillator. A calculation of this effect assuming a finite counter size is made in Chapter III. In addition, the small losses resulting from elastic scattering from ^{1}H nuclei (which are not as massive as ^{12}C nuclei and have a recoil) were neglected. It should be emphasized that these calculations were done for positive pions and are invalid for negative pions.

TABLE II

Pion Stopping Times (in Rest Frame of Pion) vs. Pion Kinetic Energy

π^+ Kinetic Energy (MeV)	Stopping Time (ns)	Probability P_3 of No Decay before Stopping
10	0.066	.997
20	0.159	.994
30	0.262	.990
40	0.368	.986
50	0.475	.982
60	0.581	.978
70	0.685	.974
80	0.787	.970
90	0.886	.967
100	0.983	.963
110	1.076	.959
120	1.167	.956
130	1.254	.953
140	1.339	.950
150	1.422	.947

TABLE III

Theoretical Efficiencies

Pion Energy (MeV)	P_1	P_2	P_3	$\varepsilon = P_1 P_2 P_3$
10	.998	.948	.997	.944
20	.991	.948	.994	.934
30	.981	.948	.990	.921
40	.967	.948	.986	.904
50	.948	.94848	.982	.882
60	.920	.948	.978	.854
70	.883	.948	.974	.815
80	.832	.948	.970	.765
90	.763	.948	.967	.699
100	.673	.948	.963	.615
110	.564	.948	.959	.513
120	.440	.948	.956	.399
130	.312	.948	.953	.282
140	.194	.948	.950	.175
150	.103	.948	.947	.092

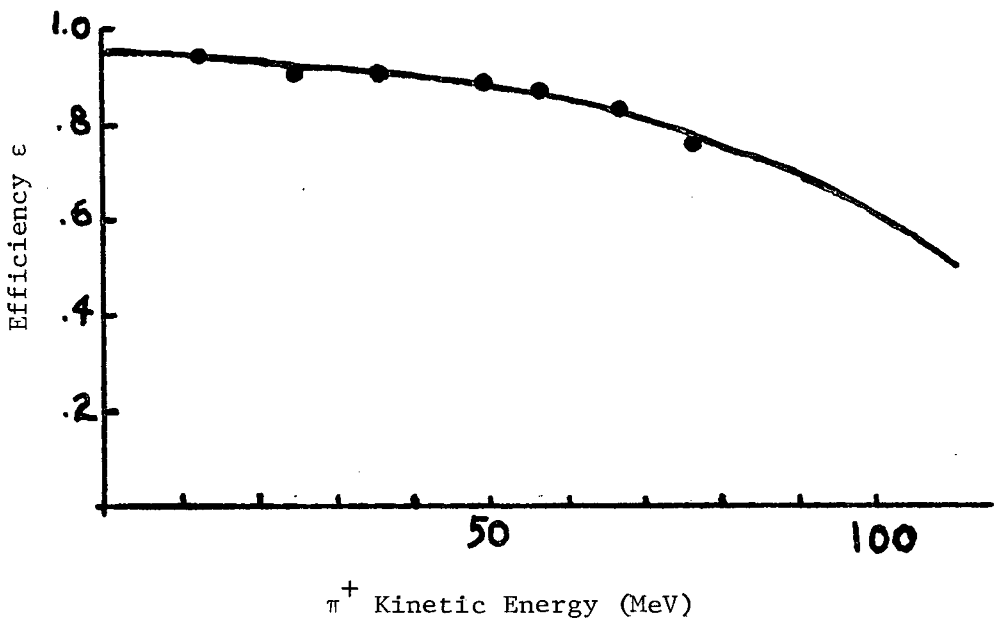

FIG. 4. Total Efficiency

CHAPTER III

CORRECTIONS TO EFFICIENCY ARISING FROM EXPERIMENTAL GEOMETRY

1. Pion Beam Contamination by Decay Muons

A Monte Carlo computer calculation of the fraction of particles entering the counter which are due to pion decays in flight was made using the following model: (see Fig. 5)

1. a pion travelling parallel to the counter axis was incident on a plane perpendicular to the direction of motion of the pion within a circle of radius R_b. The coordinates of the incident point were random variables which were generated by the computer, assuming even distribution across the circle.

2. the pion travelled a distance Z_0 before it decayed into a muon and a neutrino. The muon decayed isotropically in the centre of mass frame with lab angles θ and ϕ (spherical polar coordinates) and continued to travel in a straight line. The angles θ and ϕ were random variables generated by the computer.

3. the intersection of the trajectory of the muon and the plane Z = D (corresponding to the face of the stopping counter) was calculated. If the point of intersection lay within a circle of radius R_0 (stopping counter radius) then a "hit" was scored.

If $\vec{P}_0 = (\rho \cos \omega\vec{i} + \rho \sin \omega\vec{j} + z_0\vec{k})$ is the point of decay and $c\vec{\beta} = c\beta(\sin\theta \cos\phi\ \vec{i} + \sin\theta \sin\phi\vec{j} + \cos\theta\vec{k})$ is the muon velocity,

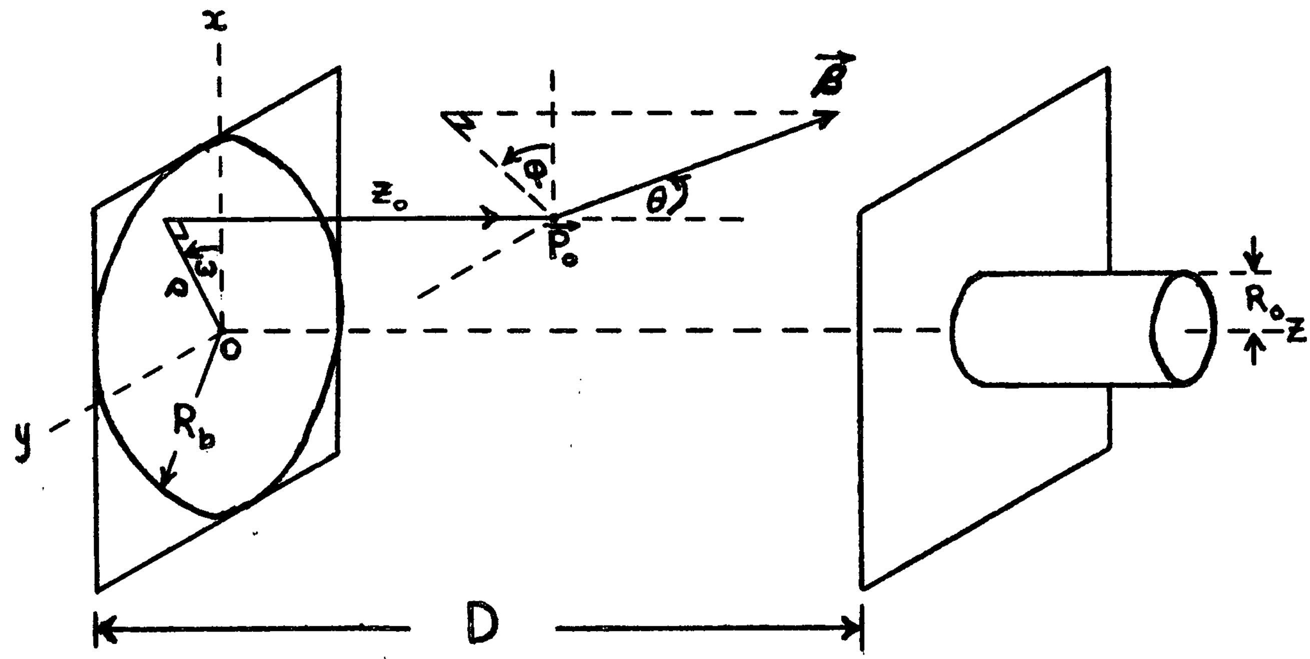

FIG. 5. Geometry for Muon Contamination Calculation

then the equation of the muon trajectory is

$$\vec{P} = \vec{P}_0 + c\vec{\beta}t \qquad \text{where } t = \text{time parameter}$$

$$\therefore \quad \vec{P} = (\rho\cos\omega + c\beta t\sin\theta\cos\varphi)\vec{i} + (\rho\sin\omega + c\beta t\sin\theta\sin\varphi)\vec{j} + (z_0 + c\beta t\cos\theta)\vec{k}$$

The muon struck the Z = D plane

when $$z_0 + c\beta t\cos\theta = D$$

$$\therefore \ c\beta t = \frac{D - z_0}{\cos\theta}$$

If $c\beta t < 0$ then the decay was in a backward direction and the muon did not intersect the Z = D plane. If $c\beta t \geq 0$ then the coordinates of the point of intersection were

$$x_s = \rho\cos\omega + \tan\theta\cos\varphi\,(D - z_0)$$

$$y_s = \rho\sin\omega + \tan\theta\sin\varphi\,(D - z_0)$$

If $x_s^2 + y_s^2 \leq R_0^2$ then a "hit" was scored.

It is assumed that the pion decay is isotropic in the centre-of-mass frame. If θ and ϕ correspond to θ^* and ϕ^* in the centre-of-mass frame then, from Appendix A,

$$\varphi = \varphi^*$$

$$\tan\theta = \frac{\beta^*\sin\theta^*}{\gamma(\beta^*\cos\theta^* + \beta_c)}$$

where $\beta^* \equiv$ muon velocity in C. of M. frame

$\beta_c \equiv$ velocity of C. of M.

$\gamma = (1-\beta_c^2)^{-1/2}$

Since the pion decays via the 2-body process, β^* is independent of angle and is equal to 0.272 (see Appendix A).

The random variables ρ, ω, Z_0, θ^* and ϕ^* were generated using the following procedure: if the distribution function to be simulated were $f(x)$ and x varied from a to b, then the cumulative distribution function

$$P = \int_a^x f(x')\,dx'$$

was calculated.

The resulting equation was solved for x. If the quantity P is given random values ranging from 0 to 1, assuming even distribution, then the resulting values of x have the desired distribution. The random numbers P were generated using the CDC 6600 subroutine RANF.

Case 1: Generation of Distributions for ρ and ω

Assuming that the probability per unit area is constant (and hence equal to $\frac{1}{\pi R_b^2}$) the probability that the incident particle strikes an area $\rho d\rho d\omega$ is

$$dP = \frac{1}{\pi R_b^2}\,\rho\,d\rho\,d\omega$$

The probability density function (PDF) in terms of the variable ρ may be found by integrating with respect to ω. Thus, the probability that the incident particle lies between ρ and ρ+dρ is

$$dP = \frac{2}{R_b^2}\,\rho\,d\rho$$

The cumulative distribution function P is thus

$$P = \int_0^\rho \frac{2}{R_b^2}\,\rho'\,d\rho' = \frac{\rho^2}{R_b^2}$$

$$\therefore\ \rho = R_b\sqrt{P}$$

Similarly, the PDF for ω is obtained by integrating with respect to ρ.

Thus,

$$dP = \frac{1}{2\pi} d\omega'$$

and

$$\omega = 2\pi P$$

Case 2: Generation of Distribution for Z_0

Assuming that the pion decays according to the exponential distribution, the PDF is then defined by

$$dP = \frac{e^{-z_0/z_m} dz_0}{z_m}$$

where $Z_m \equiv$ mean decay length of pion

(varies with pion energy)

Then,

$$P = \int_0^{z_0} \frac{e^{-z_0'/z_m} dz_0'}{z_m} = 1 - e^{-z_0/z_m}$$

$$\therefore z_0 = -z_m \ln(1-P)$$

Case 3: Generation of Distribution for θ^* and ϕ^*

Assuming that the probability of decay per unit solid angle is constant (and hence equal to $\frac{1}{4\pi}$) the PDF is defined by

$$dP = \frac{1}{4\pi} \sin\theta^* d\theta^* d\varphi^*$$

Integrating out the variable ϕ^*,

$$dP = \frac{1}{2} \sin\theta^* d\theta^*$$

$$\therefore \quad P = \int_0^{\theta^*} \frac{1}{2} \sin\theta^{*\prime} d\theta^{*\prime} = \frac{1}{2}(1-\cos\theta^*)$$

$$\therefore \quad \cos\theta^* = (1-2P)$$

Integrating out θ^*,

$$dP = \frac{1}{2\pi}\, d\varphi^{*\prime},$$

$$\varphi^* = 2\pi P$$

Calculations of the ratio of muons striking the target to total particles (pions and muons) striking the target were made for various pion energies and are shown in Table IV. For these calculations D = 400 cm (distance between bending magnet H2 and counter), R_b = 6 cm and R_0 = 4 cm.

TABLE IV

Muon Contamination of Pion Beam

Pion Energy (MeV)	Mean Decay Distance (cm)	Mu's/Total
10	301	.042
20	433	.040
30	539	.043
40	632	.040
50	718	.044
60	798	.042
70	875	.042
80	948	.041

2. Elastic Scattering Out of Scintillator

Both Coulomb scattering and nuclear elastic scattering were considered. Using formulas for multiple Coulomb scattering (see, for example, "Techniques of High Energy Phyiics", edited by D.M. Ritson, pp. 7-11[10]) the root mean square lateral spread of a beam of 80 MeV pions which pass through a slab of CH_2 of thickness 17.7 gcm^{-2} was calculated to be <1 cm. As the range of 80 MeV pions in CH_2 is 18.2 gcm^{-2}, a scintillator of 5" diameter is sufficiently large to contain all 80 MeV pions undergoing Coulomb scattering.

The effect of nuclear scattering is more significant, however, as the scattering distributions are generally less peaked in the forward direction than in the case of Coulomb scattering. The assumption was made that nuclear scattering was isotropic and a calculation of the nuclear elastic scattering out of a cylindrical scintillator of radius R_0 = 6.35 cm and length L = 30.5 cm was made using a computerized Monte Carlo procedure; in addtion, a finite incident beam of pions was assumed (see Fig. 6). The following model was used:

1. a pion travelling along a line parallel to the counter axis struck the counter at a random point lying within a circle of radius R_b = 4 cm. A uniform distribution across the area was assumed.

2. the pion continued to travel through the scintillator until it stopped or scattered elastically (nuclear scattering only). A mean free path length of 60 cm was used to generate a random scattering distance; the mean free path was calculated using an average cross section of 300 mb for ^{12}C and 50 mb for ^{1}H.

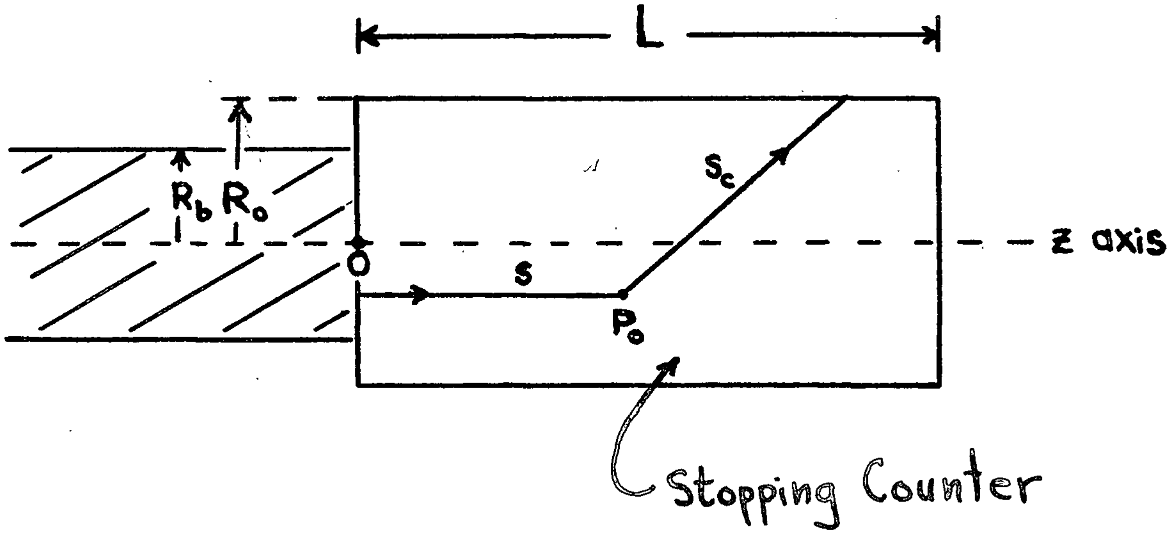

FIG. 6. Geometry for Elastic Scattering Calculation

3. if scattering occurred, the coordinates of the scattering centre P_0 and the pion energy at P_0 were calculated. The random scattering angles θ and ϕ (in spherical polar coordinates) were generated and the distance S_c between P_0 and the intersection of the straight line trajectory of the scattered pion with the boundary of the scintillator was calculated.

4. another random scattering distance was generated; if scattering occurred then step 3 was repeated; if not, then the distance S_c was compared to the pion range to determine whether the pion escaped the scintillator.

A flow diagram for the computer programme which performed the above calculation is shown in Fig. 7. The methods of generating the various random variables are the same as those described earlier. The distribution of the scattering distance s was assumed to be exponential with the mean free path corresponding to the mean value of s. The calculation of the distance to the scintillator boundary S_c is described in Appendix B.

The results of the calculation are shown in Table V; they should be considered as upper limits only, as the mean free path was underestimated.

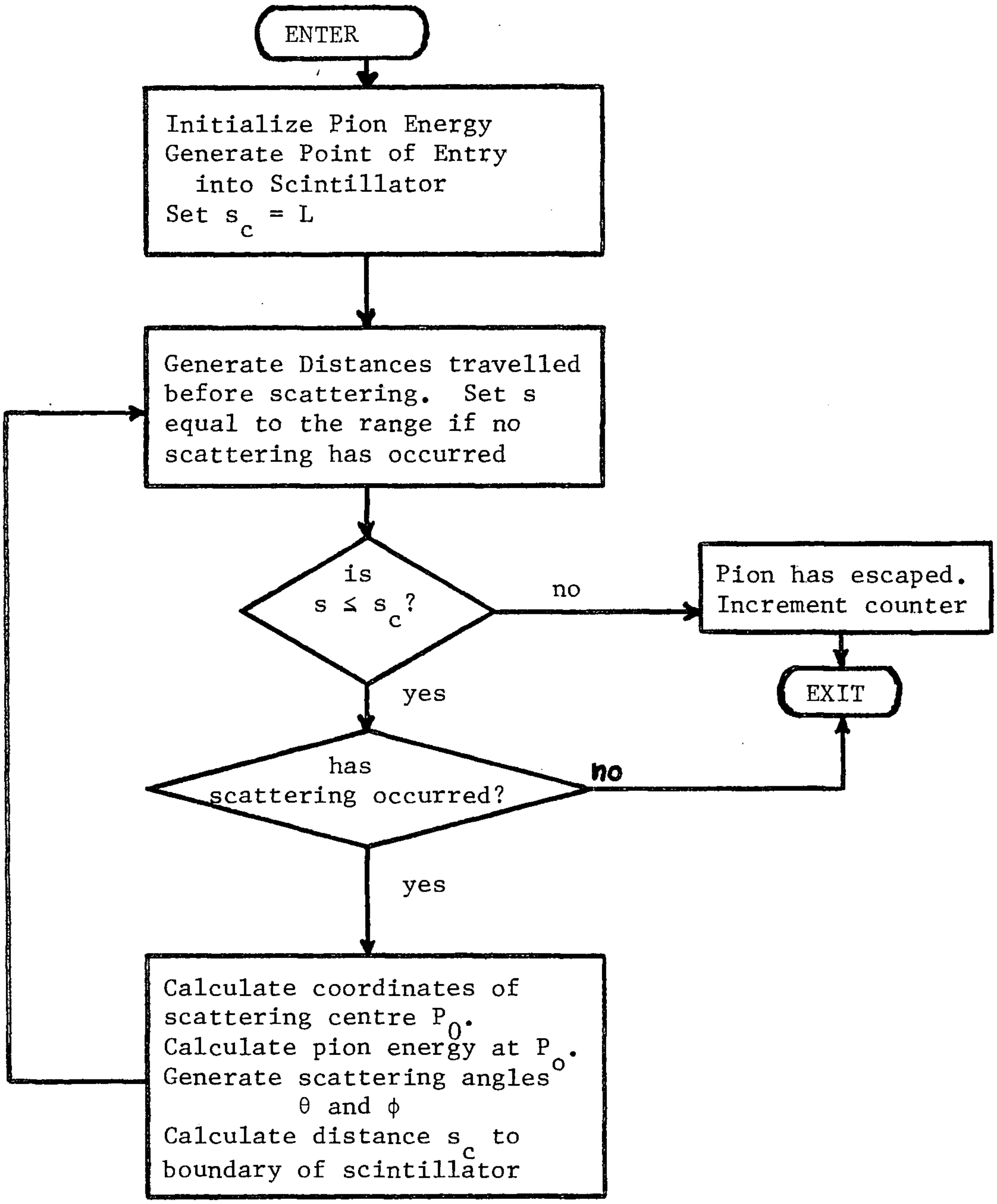

FIG. 7. Flow Diagram for Elastic Scattering Calculation

TABLE V

Elastic Scattering out of Scintillator

Pion Energy (MeV)	Pion Range in Scintillator (cm)	Scattered Pions/Total
20	1.9	<.0001
30	4.0	.0005
40	6.7	.0054
50	11.2	.049
60	14.0	.086
70	18.5	.14
80	23.6	.20

CHAPTER IV

EFFICIENCY MEASUREMENTS

1. Experimental Arrangement

The arrangement is depicted schematically in Fig. 8. A polythene target placed in the primary proton beam of the 184" cyclotron at the Lawrence Berkeley Laboratory was used to produce positive pions. The pion beam was passed through bending magnet H1 to remove undesired particles such as scattered protons, negative pions and electrons. Beam focussing was effected by 2 pairs of quadrupole magnets (Q1, Q2, Q3 and Q4) and a second bending magnet H2 selected pions of the desired momentum. A final quadrupole magnet Q5 provided additional focussing in the horizontal plane.

Scintillation counters B1, B2, B3 and B4, each made up of pieces of 15 cm x 10 cm NE102 plastic scintillator of 0.5 cm thickness, defined the pion beam. The time of flight between B1 and B2 (path length approximately 6m) enabled identification of particle type. A hodoscope array of 12 NE102 plastic scintillation counters, each of dimensions 20 cm x 1 cm x 0.2 cm thickness, defined the incident momentum of the particles. With the pion beam defined in this manner, the pion flux was $\sim 1 \times 10^4$/sec for 50 MeV pions. The pion flux as a function of energy is shown in Fig. 9. An event, defined by a B1-B2-B3-B4-C1 coincidence, gave an interrupt signal to a NOVA 1200 computer (12K memory). A data acquisition programme developed at the University of British Columbia[(11)] was used to read the contents of CAMAC scalers which contained information from the spark chambers, hodoscope, stopping counter analogue-to-digital-converter (ADC) and B1 $\rightarrow$ B2 time-of-flight encoder.

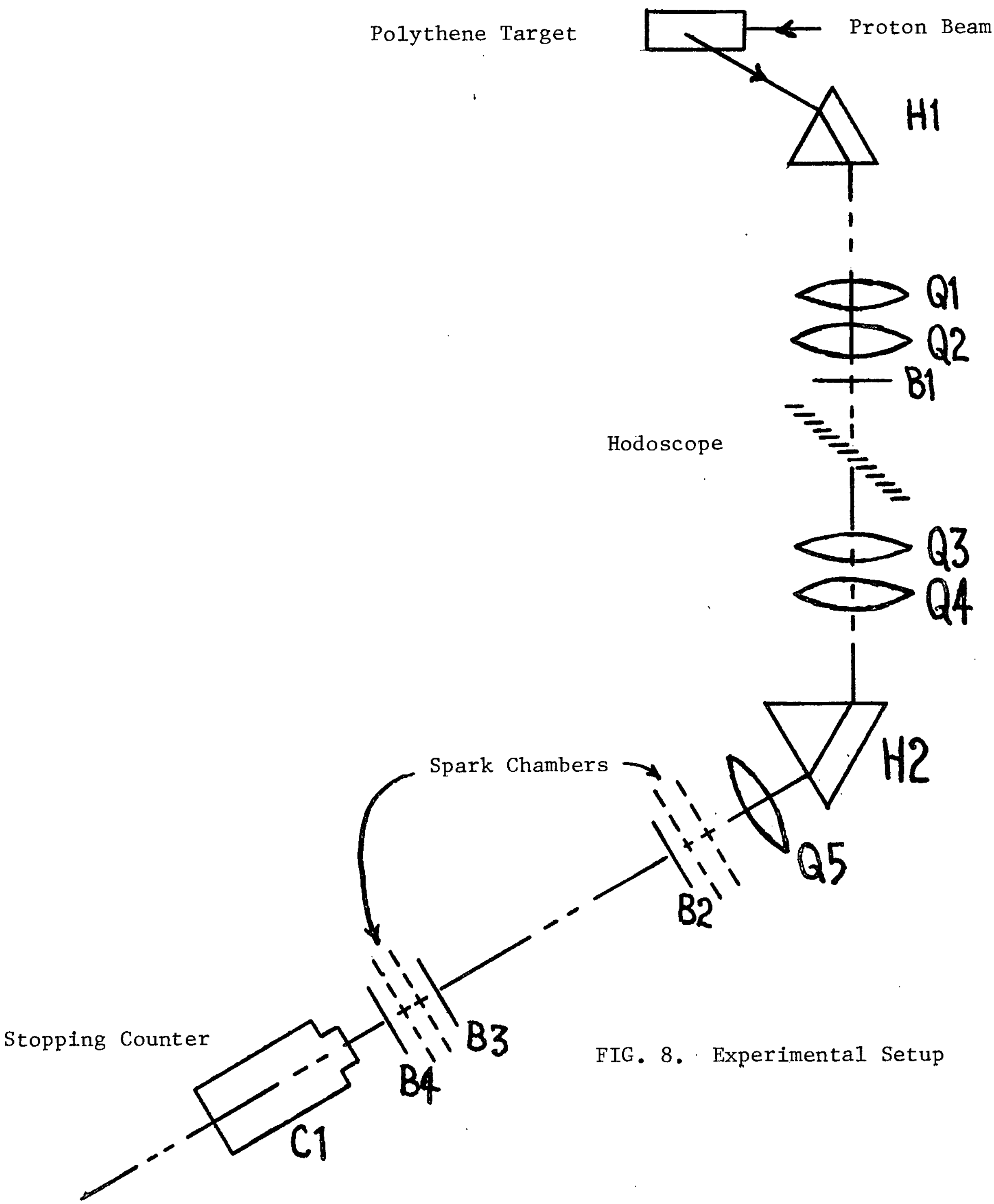

FIG. 8. Experimental Setup

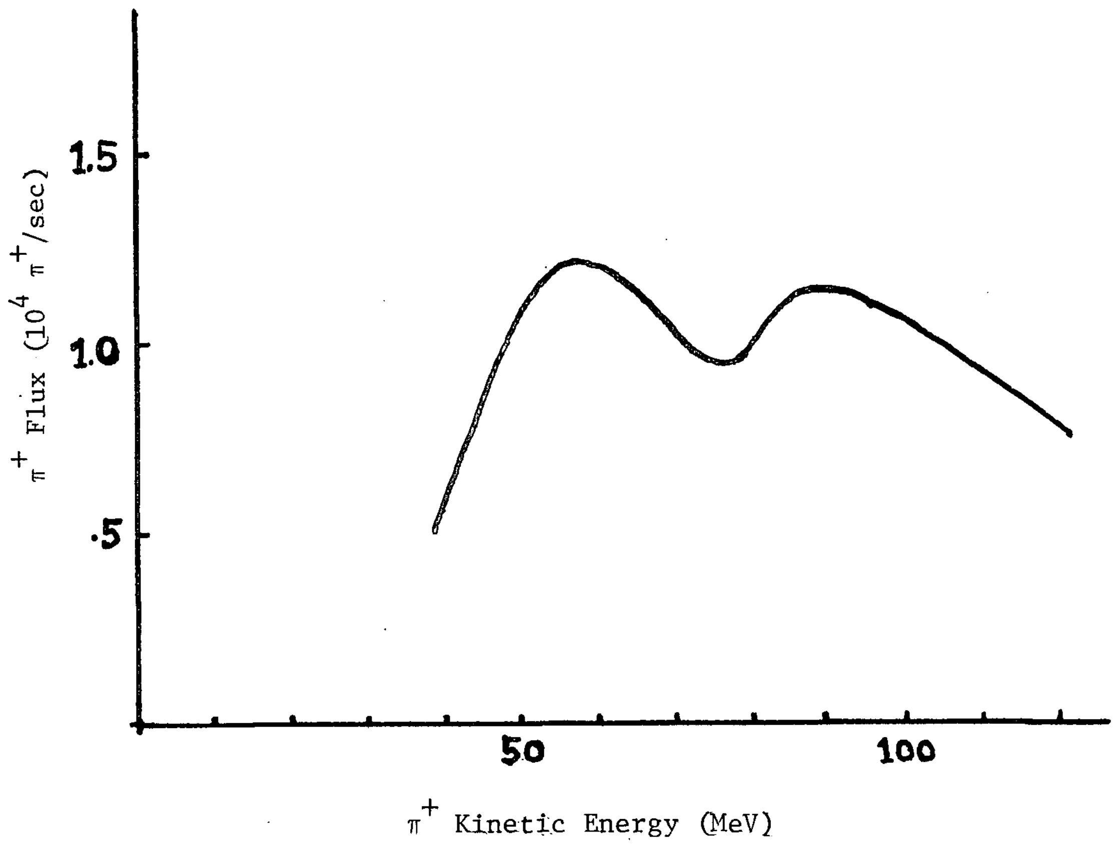

FIG. 9. Pion Flux vs. Energy

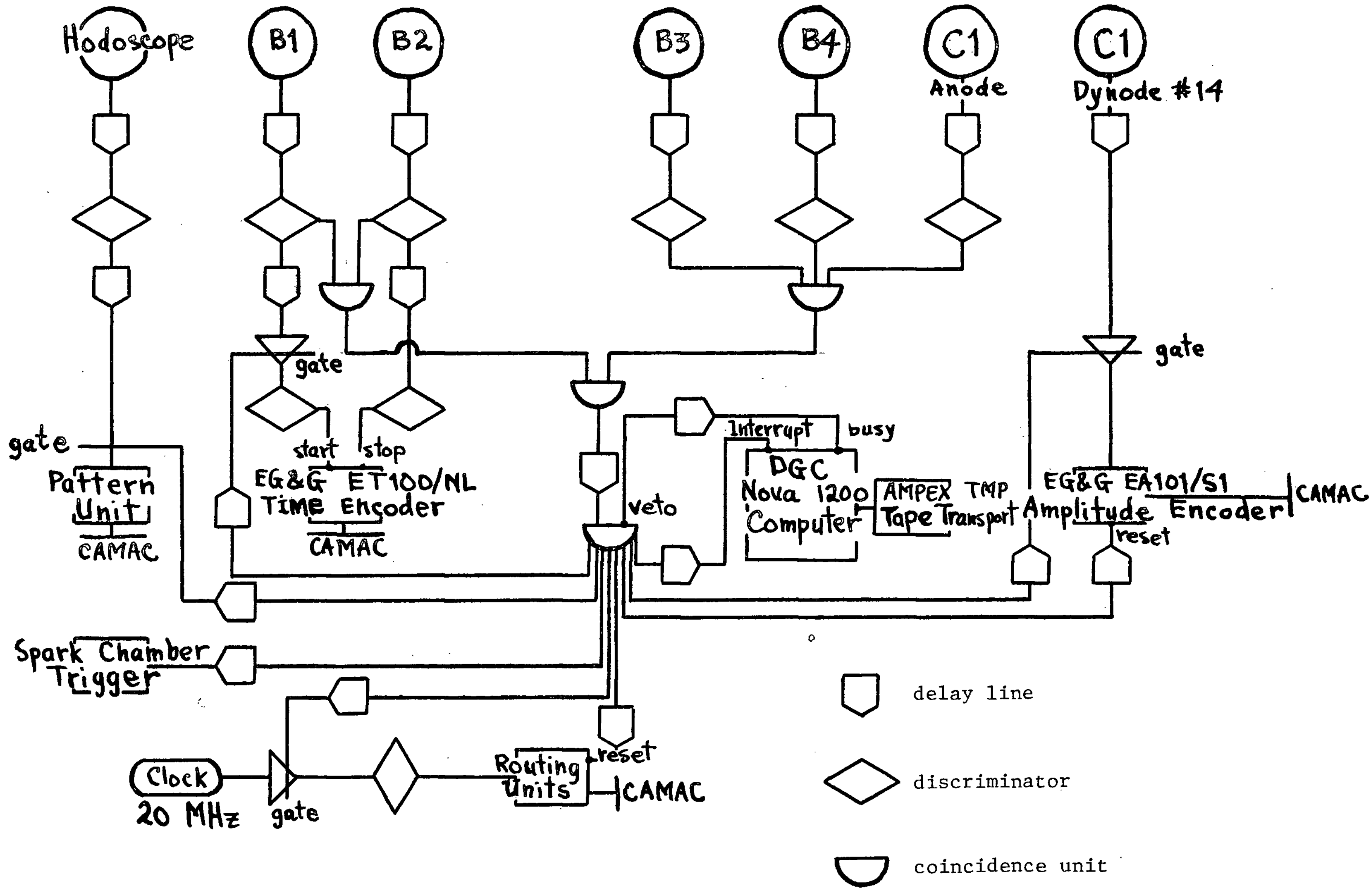

FIG. 10. Experiment Logic

This data was then transferred from the computer memory to magnetic tape for off-line analysis. Each 2400-ft. reel of tape was able to hold information on 80,000 events.

2. Data Analysis

Histograms of the ADC spectra at various pion energies were made using a general purpose computer programme developed by W. Westlund at U.B.C. In order to obtain unbiased efficiency measurements only those events satisfying the following criteria were considered in the analysis:

1. The particle passed through the centre region of the hodoscope
2. the angle between the two particle trajectories defined by the 2 pairs of spark chambers was <0.1 radians
3. the time of flight between B1 and B2 fell between narrow limits to ensure positive identification of the pion. Figure 11 shows a typical time encoder spectrum at 49 MeV. The limits indicated by the vertical lines served to identify the pion.
4. the pion was incident upon the face of the stopping counter and within a concentric circle of radius 4 cm.

Restrictions 2 and 3 eliminated some of the decay muon contamination, as a fraction of the pion decays occurred downstream of bending magnet H2 would result in non-collinear trajectories and in flight times slightly different from that of the pions. Upper limits to the remaining

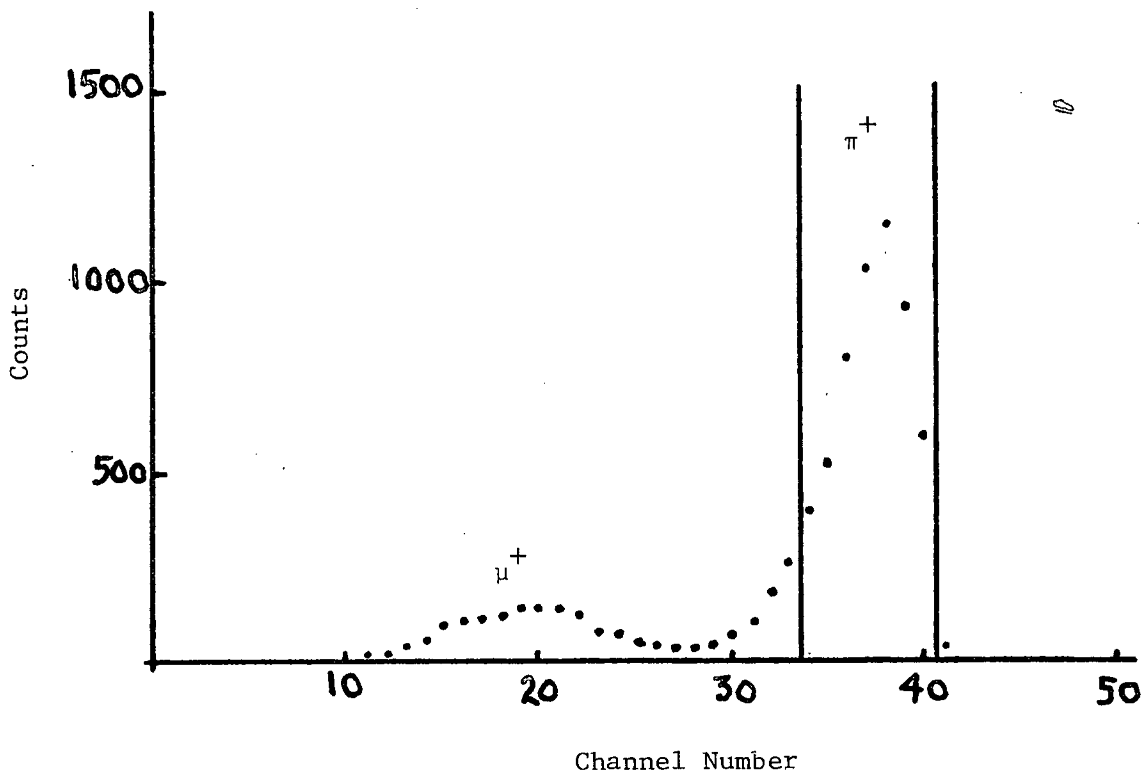

FIG. 11. Typical Time Encoder Spectrum at 49 MeV

muon contamination were given in Chapter III. Examples of typical ADC spectra associated with 49 MeV pions before and after application of the restrictions are shown in Figs. 12 and 13. The overlapping muon and pion peaks were clearly separated. Pion spectra after restrictions are shown for various pion energies in Figs. 14 to 19.

Efficiencies were obtained by integrating the peak and dividing by the total counts in the spectrum. The 10 lowest channels in the spectrum corresponding to pulses below 80 mV threshhold of the discriminator connected to C1 anode (see Fig. 10) were assumed to contain no bona fide pion events. The experimental efficiencies are given in Table VI and are plotted in Fig. 4.

Peak Integration

The following procedure was used:

1. the peak centroid was calculated using the formula

$$\bar{x} = \frac{\sum_{i=1}^{n} y_i x_i}{\sum_{i=1}^{n} y_i}$$

where $x_i \equiv$ channel number

$y_i \equiv$ counts in channel i

$n \equiv$ no. of channels

Substituting $x_i = x_1 + i-1$, where x_1 is the number of the 1^{st} channel, in the above equation:

$$\bar{x} = x_1 - 1 + \frac{\sum_{i=1}^{n} y_i i}{Y}$$

where $Y = \sum_{i=1}^{n} y_i$

2. the standard deviation σ of the peak was then calculated from

$$\sigma^2 = \frac{\sum_{i=1}^{n} y_i (x_i - \bar{x})^2}{Y}$$

Substituting the expressions for x_i and $\bar{x}$,

$$\sigma^2 = \frac{\sum_{i=1}^{n} y_i i^2}{Y} - \left(\frac{\sum_{i=1}^{n} y_i i}{Y} \right)^2$$

3. the peak was assumed to be Gaussian and was summed from $\bar{x} - 2.5\sigma$ to $\bar{x} + 2.5\sigma$. The result was divided by 0.9876 (the area under the Gaussian curve from -2.5σ to 2.5σ) to obtain the result.

TABLE VI

Experimental Efficiencies

Pion Momentum At Magnet H2 (MeV/c)	Pion Kinetic Energy (MeV)*	Efficiency	Error %
78	12.0	.939	0.7
96	24.3	.909	0.7
114	35.3	.909	0.5
133	49.1	.887	0.6
143	56.3	.870	0.7
157	66.5	.827	0.8
170	76.8	.792	0.7

*Corrected for energy loss in material placed in beam line

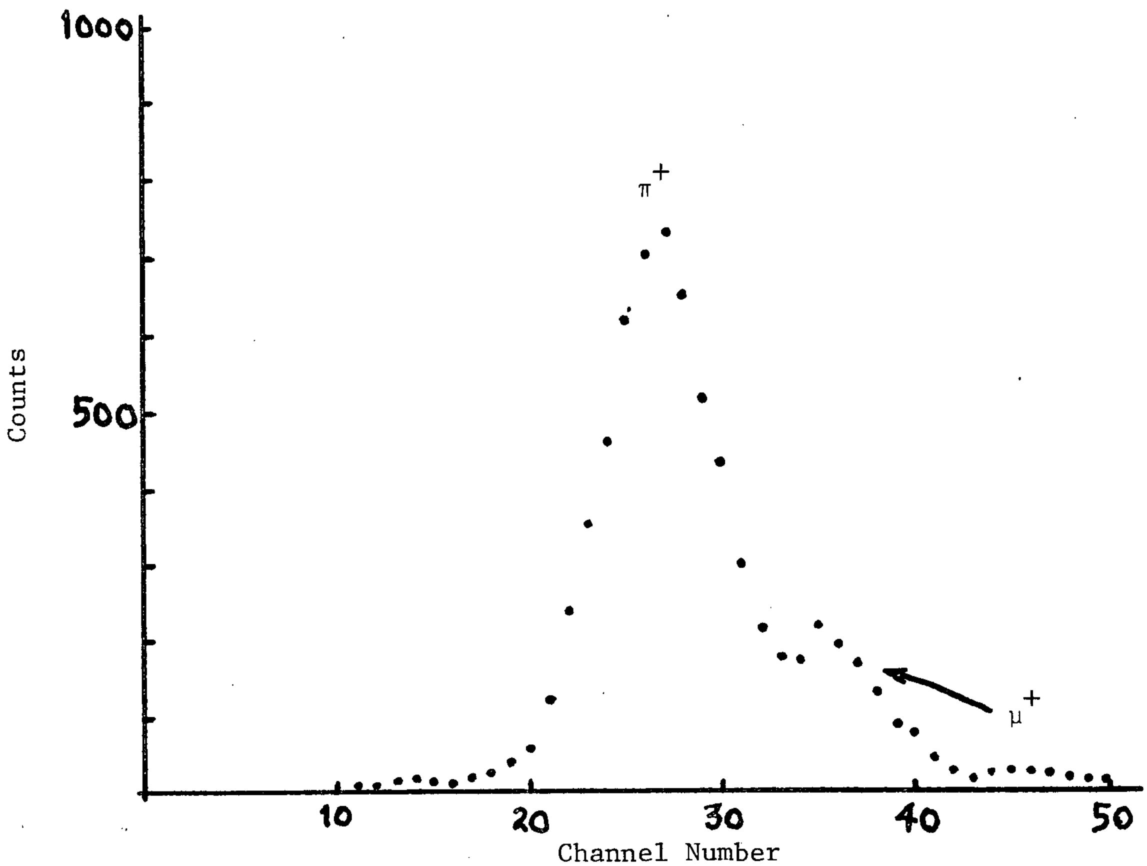

FIG. 12. ADC Spectrum at 49 MeV before Restrictions

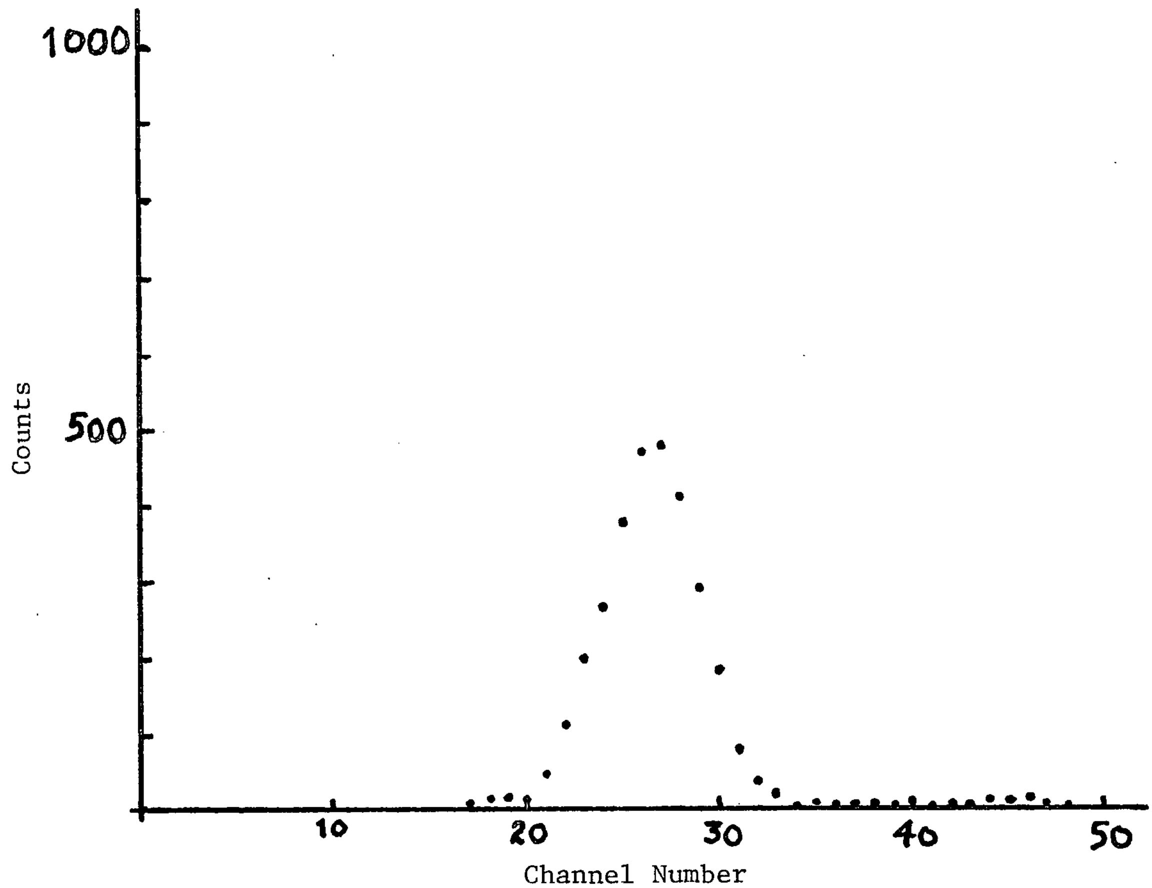

FIG. 13. ADC Spectrum at 49 MeV after Restrictions

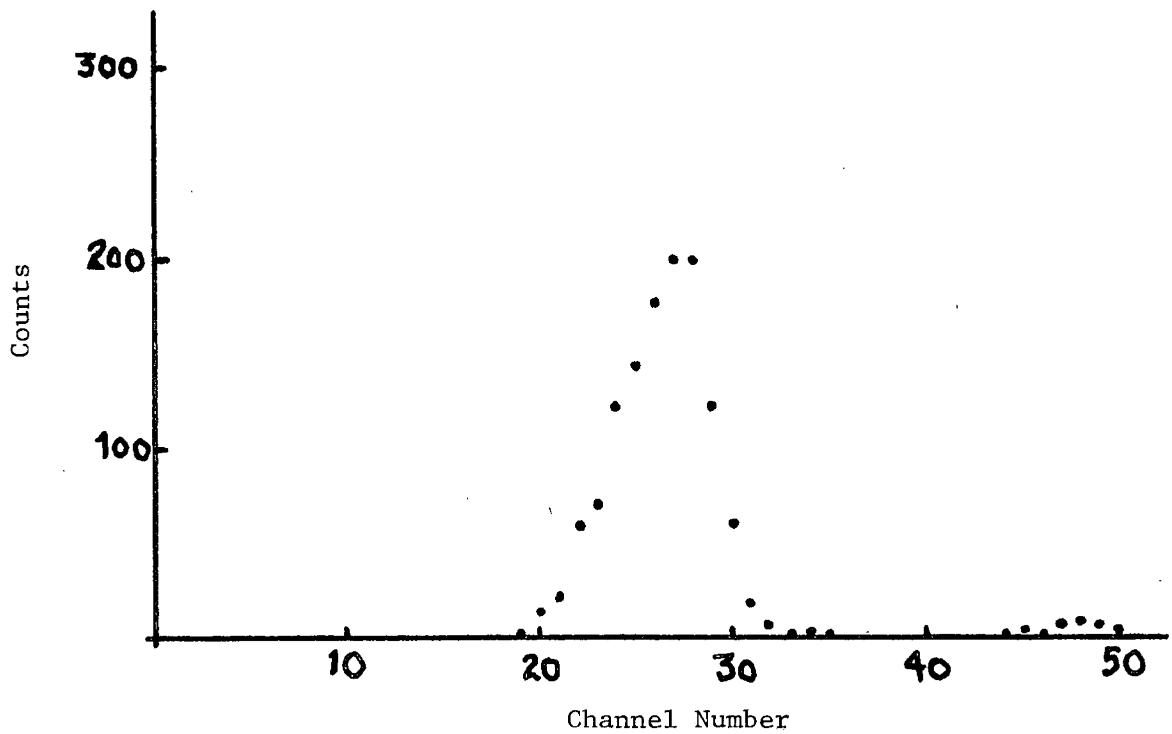

FIG. 14. ADC Spectrum at 12 MeV

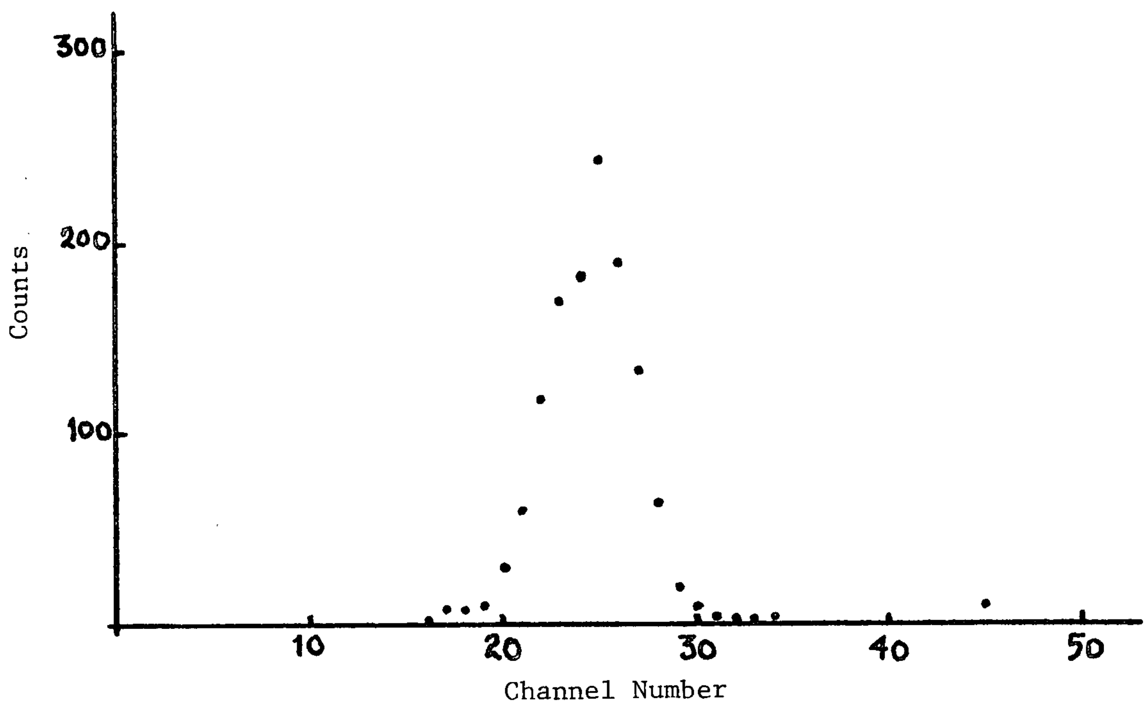

FIG. 15. ADC Spectrum at 24 MeV

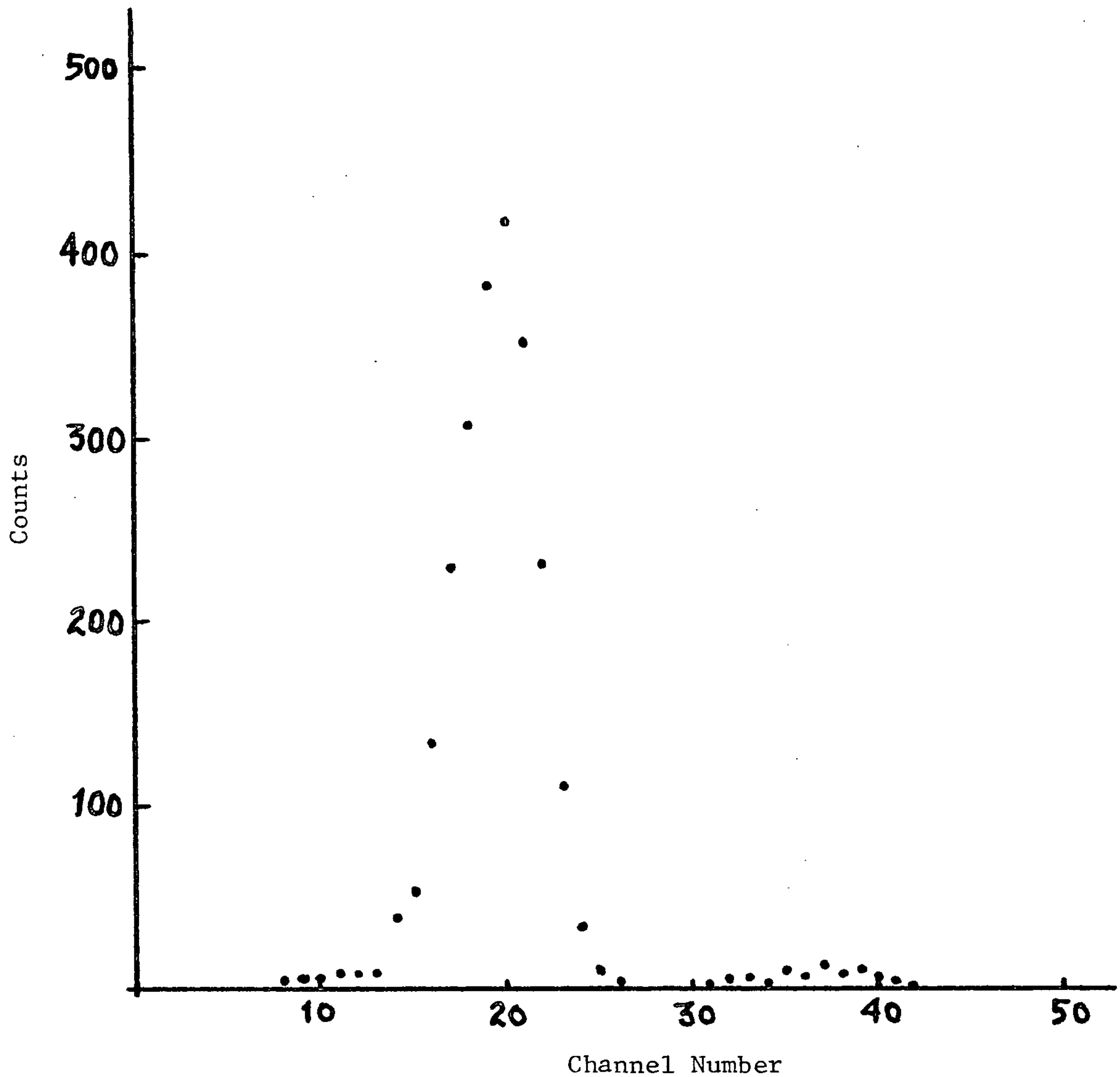

FIG. 16. ADC Spectrum at 35 MeV

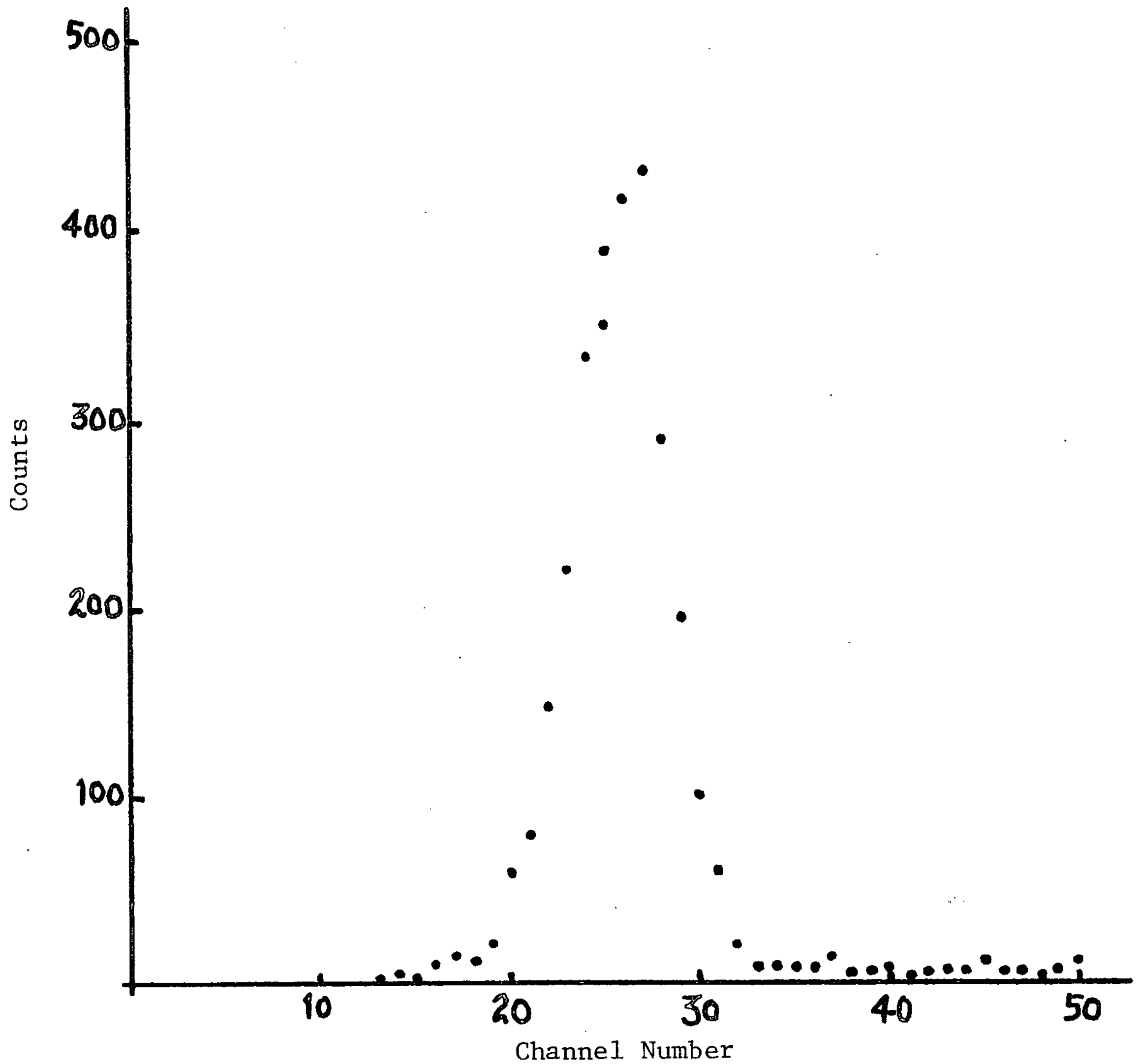

FIG. 17. ADC Spectrum at 56 MeV

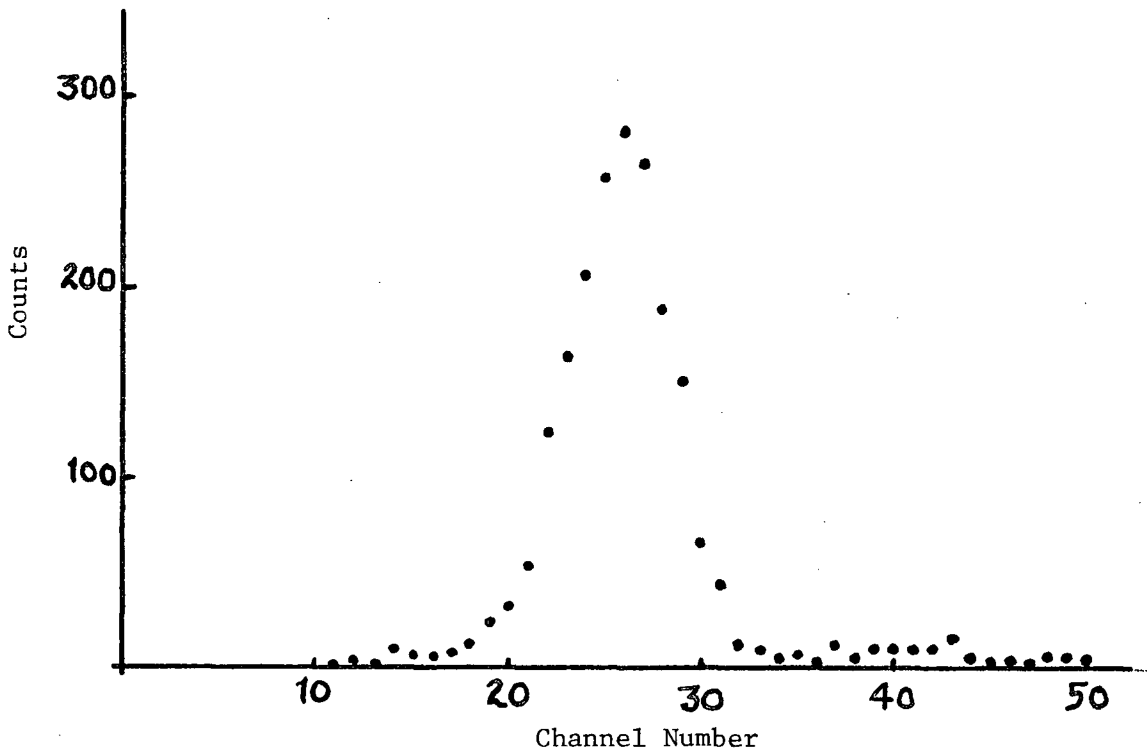

FIG. 18. ADC Spectrum at 67 MeV

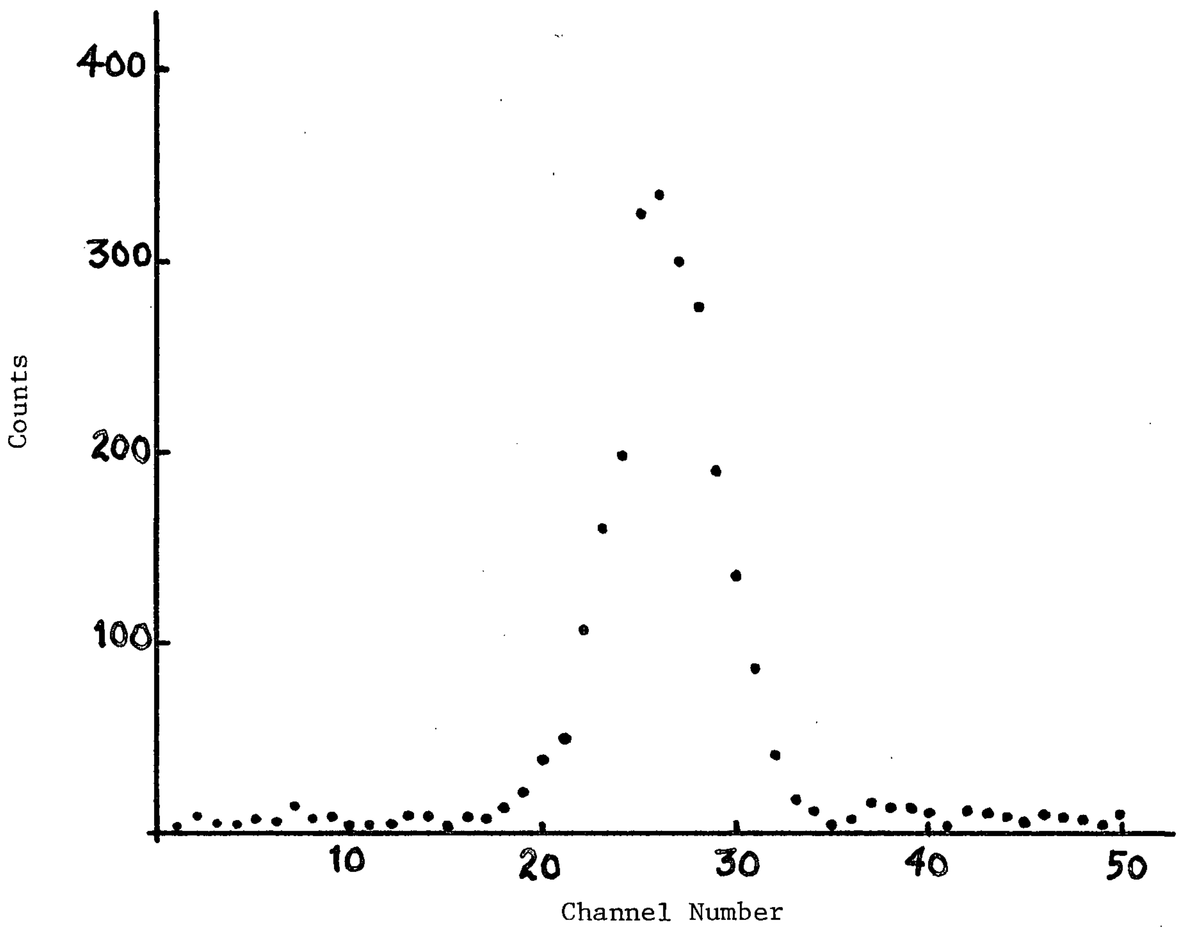

FIG. 19. ADC Spectrum at 77 MeV

CHAPTER V

CONCLUSIONS

The processes described in Chapter II account for the observed efficiency; the energy dependence of the efficiency is due largely to the effect of inelastic reactions in the scintillator. The inelastic reactions limit the usefulness of stopping counters to pion energies of 100 MeV or less. The efficiency is relatively insensitive to the duration of the gate length beyond 120 ns, as is seen in Fig. 3.

The good agreement between theory and experiment at low energies, where the effect of inelastic reactions is not prominent, indicates that the time of flight and spatial restrictions imposed for the experimental determination of the efficiency served to reduce contamination of the pion beam by decay muons to negligible amounts. The effects of nuclear elastic scattering out of the scintillator appear to be much smaller than the worst case-estimates.

BIBLIOGRAPHY

1. D.F. Measday and C. Richard-Serre, CERN 69-17.

2. D.F. Measday and C. Richard-Serre, Nuclear Instruments and Methods 76 45 (1969).

3. H. Bethe, Annalen der Physik 5 325 (1930).

4. CRC Handbook of Chemistry and Physics (49th Edition).

5. TRIUMF Kinematics Handbook.

6. D. Stork, Physical Review 93 868 (1954).

7. R.L. Martin, Physical Review 87 1052 (1952).

8. Nuclear Enterprises Catalogue (1970).

9. "Review of Particle Properties", Reviews of Modern Physics, Vol. 43, No. 2, Part II, April 1971.

10. "Interscience Monographs and Texts in Physics and Astronomy", edited by R. Marshak, Vol. V - "Techniques of High Energy Physics", edited by D. Ritson, Interscience Publishers Inc., 1961.

11. D. Lepatourel and R. Johnson, "A Data Acquisition System Based on CAMAC and Supported by BASIC and FORTRAN" (Submitted to the CAMAC Bulletin).

APPENDIX A

$\pi^+ \rightarrow \mu^+$ DECAY KINEMATICS

1) Energy of Decay Muon

Pions decay via the reaction

$$\pi^+ \longrightarrow \mu^+ + \nu_\mu \quad .$$

A pion travelling in a certain direction with total energy E_π decays into a muon and neutrino. The muon flies off at an angle θ from the pion direction and has total energy E_μ.

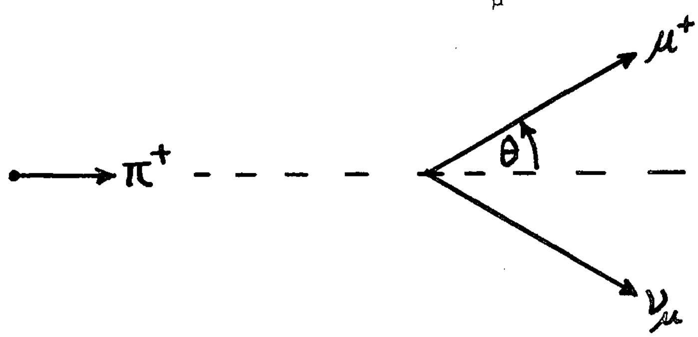

Using the 4-vector notation of Special Relativity, the conservation of momentum is written as

$$\vec{p}_\pi = \vec{p}_\mu + \vec{p}_\nu$$

where

$\vec{p} = (P, iE)$

$\vec{P} \equiv$ ordinary 3 dimensional momentum

$E \equiv$ total energy

$i^2 \equiv -1$

$$\vec{p}_\nu \cdot \vec{p}_\nu = \vec{p}_\pi \cdot \vec{p}_\pi + \vec{p}_\mu \cdot \vec{p}_\mu - 2\vec{p}_\pi \cdot \vec{p}_\mu$$

$$P_\nu^2 - E_\nu^2 = P_\pi^2 - E_\pi^2 + P_\mu^2 - E_\mu^2 - 2(\vec{P}_\pi \cdot \vec{P}_\mu - E_\pi E_\mu)$$

But $E^2 = P^2 + m^2$ where m ≡ mass in MeV

$$\therefore \; -m_\nu^2 \equiv 0 = -m_\pi^2 - m_\mu^2 - 2P_\pi P_\mu \cos\theta + 2E_\pi E_\mu$$

$$2P_\pi P_\mu \cos\theta = 2E_\pi E_\mu - (m_\pi^2 + m_\mu^2)$$

Squaring,

$$4P_\pi^2 P_\mu^2 \cos^2\theta = 4E_\pi^2 E_\mu^2 - 4(m_\pi^2 + m_\mu^2)E_\pi E_\mu + (m_\pi^2 + m_\mu^2)^2$$

$$\text{or,} \quad 4(E_\pi^2 - m_\pi^2)(E_\mu^2 - m_\mu^2)\cos^2\theta = \text{R.H.S.}$$

But $E_\pi = \gamma m_\pi$ where $\gamma = (1-\beta^2)^{-1/2}$

Substituting in above equations and solving for E_μ:

$$E_\mu = \frac{\gamma(m_\pi^2 + m_\mu^2) \pm \cos\theta\sqrt{\gamma^2-1}\sqrt{(m_\pi^2+m_\mu^2)^2 - 4m_\pi^2 m_\mu^2(\gamma^2\sin^2\theta + \cos^2\theta)}}{2m_\pi(\gamma^2\sin^2\theta + \cos^2\theta)}$$

If the pion is initially at rest, $\gamma = 1$. Thus

$$E_\mu = \frac{m_\pi^2 + m_\mu^2}{2m_\pi}$$

The kinetic energy T_μ and the velocity β^* (in units of c) are thus

$$T_\mu = \frac{(m_\pi - m_\mu)^2}{2m_\pi} \qquad \beta^* = \frac{m_\pi^2 - m_\mu^2}{m_\pi^2 + m_\mu^2}$$

Using m_π = 139.576 MeV and m_μ = 105.6594 MeV, T_μ = 4.16 MeV and β^* = 0.272.

2) Transformation of Muon Angle from Centre of Mass to Lab Frame

Let the z-axis be parallel to the direction of motion of the pion.

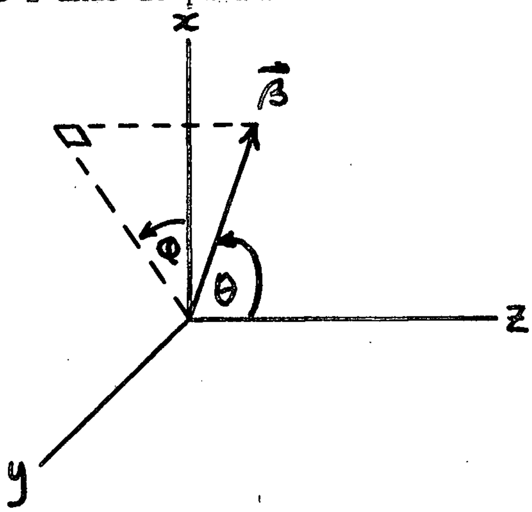

$\vec{\beta}$ ≡ velocity (in units of c) of decay muon in lab frame.

The Lorentz transformation between a rest frame and a frame moving along the z-axis with velocity β_c (in units of c) in matrix notation is

$$\begin{bmatrix} x \\ y \\ z \\ ct \end{bmatrix} = \begin{bmatrix} 1 & 0 & 0 & 0 \\ 0 & 1 & 0 & 0 \\ 0 & 0 & \gamma & \beta_c\gamma \\ 0 & 0 & \beta_c\gamma & \gamma \end{bmatrix} \cdot \begin{bmatrix} x^* \\ y^* \\ z^* \\ ct^* \end{bmatrix}$$

where $\gamma = (1-\beta_c^2)^{-1/2}$

The asterisks refer to quantities in the moving frame. The resulting 4 equations are

$$x = x^*$$

$$y = y^*$$

$$z = \gamma z^* + \beta_c \gamma c t^*$$

$$ct = \beta_c \gamma z^* + \gamma c t^*$$

$$\beta_x = \frac{1}{c}\frac{dx}{dt} = \frac{dx^*}{\beta_c \gamma\, dz^* + \gamma c\, dt^*} = \frac{\frac{1}{c}\frac{dx^*}{dt^*}}{\beta_c \gamma \left(\frac{1}{c}\right)\frac{dz^*}{dt^*} + \gamma}$$

$$= \frac{\beta_x^*}{\gamma(1+\beta_c \beta_z^*)}$$

Similarly,

$$\beta_y = \frac{\beta_y^*}{\gamma(1+\beta_c \beta_z^*)}$$

and

$$\beta_z = \frac{\beta_z^* + \beta_c}{1+\beta_c \beta_z^*}$$

Using spherical polar coordinates, these are expressed as

$$\beta \sin\theta \cos\varphi = \frac{\beta^* \sin\theta^* \cos\varphi^*}{\gamma(1+\beta_c \beta^* \cos\theta^*)}$$

$$\beta \sin\theta \sin\varphi = \frac{\beta^* \sin\theta^* \sin\varphi^*}{\gamma(1+\beta_c \beta^* \cos\theta^*)}$$

$$\beta \cos\theta = \frac{\beta^* \cos\theta^* + \beta_c}{1+\beta_c \beta^* \cos\theta^*}$$

Dividing the 2nd by the 1st

$$\tan\varphi = \tan\varphi^*$$

or

$$\varphi = \varphi^*$$

Dividing the 2nd by the 3rd ($\sin\varphi = \sin\varphi^*$):

$$\tan\theta = \frac{\beta^* \sin\theta^*}{\gamma(\beta^* \cos\theta^* + \beta_c)}$$

APPENDIX B

DISTANCE S_c BETWEEN SCATTERING CENTRE P_0 AND BOUNDARY OF DETECTOR (see Fig. 6)

The equation of the scattered pion is

$$\vec{p} = \vec{p}_0 + S\vec{n}$$

where $\vec{p}_0 = x_0\vec{i} + y_0\vec{j} + z_0\vec{k}$

and $\vec{n}$ is a unit vector in the direction of scattering;

i.e. $\vec{n} = \sin\theta\cos\varphi\,\vec{i} + \sin\theta\sin\varphi\,\vec{j} + \cos\theta\,\vec{k}$

S = distance parameter

$$\therefore \vec{P} = (x_0 + S\sin\theta\cos\varphi)\vec{i} + (y_0 + S\sin\theta\sin\varphi)\vec{j} + (z_0 + S\cos\theta)\vec{k} \qquad (8)$$

The trajectory of the scattered pion intersects either a) the front face b) the rear face or c) the cylindrical wall.

cylindrical wall.

Possibility 1: Exit through front face

The straight line given by eq. 8 intersects the front face if

$$z_0 + S\cos\theta = 0$$

$$\therefore S = -\frac{z_0}{\cos\theta}$$

If S < 0 then the scattering is in the forward direction and the pion cannot intersect the front face. If S > 0 then intersection with the front face is possible. The coordinates of the point of intersection are

$$x_s = x_0 + S \sin\theta\cos\phi$$

$$y_s = y_0 + S \sin\theta\sin\phi$$

If $x_s^2 + y_s^2 \leq R_0^2$ then the trajectory intersects with front face and

$$S_c = -\frac{z_0}{\cos\theta};$$

otherwise intersection occurs with the scintillator wall.

Possibility 2: Exit through rear face

The straight line from eq. (8) intersects the rear face if

$$z_0 + S\cos\theta = L$$

$$\therefore S = \frac{L - z_0}{\cos\theta}$$

If S < 0 then intersection occurs with the wall. If S $\geq$ 0 then the procedure outlined in possibility 1 determines whether intersection with the rear face occurs. If so, then

$$S_c = \frac{L - z_0}{\cos\theta}$$

Possibility 3: Exit through side

The point of intersection is such that

$$(x_0 + S\sin\theta\cos\varphi)^2 + (y_0 + S\sin\theta\sin\varphi)^2 = R_0^2$$

Solving for S,

$$S = \frac{-(x_0 \cos\varphi + y_0 \sin\varphi) \pm \sqrt{R_0^2 - (x_0 \sin\varphi - y_0 \cos\varphi)^2}}{\sin\theta}$$

the positive solution is chosen, so that

$$S_c = \frac{\sqrt{R_0^2 - (x_0 \sin\varphi - y_0 \cos\varphi)^2} - (x_0 \cos\varphi + y_0 \sin\varphi)}{\sin\theta}$$